

Anisotropic Thermal Conductivity of Ge Quantum-Dot and Symmetrically Strained Si/Ge Superlattices

W. L. Liu,^a T. Borca-Tasciuc,^a G. Chen,^{a,*} J. L. Liu,^b and K. L. Wang^b

^a*Nanoscale Heat Transfer and Thermoelectrics Laboratory, Mechanical and Aerospace Engineering Department, University of California, Los Angeles, California 90095, USA*

^b*Device Research Laboratory, Electrical Engineering Department, University of California, Los Angeles, California 90095, USA*

We report the first experimental results on the temperature dependent in-plane and cross-plane thermal conductivities of a symmetrically strained Si/Ge superlattice and a Ge quantum-dot superlattice measured by the two-wire 3ω method. The measured thermal conductivity values are highly anisotropic and are significantly reduced compared to the bulk thermal conductivity of the structures. The results can be explained by using heat transport models based on the Boltzmann transport equation with partially diffusive scattering of the phonons at the superlattice interfaces.

Keywords: Thermal Conductivity, Ge Quantum Dot, Si/Ge Superlattices, Anisotropy.

Low-dimensional semiconductor superlattices are widely used in electronics and optoelectronics. Investigation of heat transport in superlattices is very important for thermal control and device operations.¹ Recently, it was shown that the thermoelectric figure of merit can be increased in low-dimensional materials through size effects to enhance the electron performance^{2–4} and to reduce the phonon thermal conductivity.^{5,6} These applications have led to quite a few experimental investigations on the thermal conductivity of superlattices of different material systems.^{7–16} In the theoretical aspect, several approaches that considering group velocity modification and phonon confinement based on lattice dynamics models,^{7–22} diffuse interface scattering based on Boltzmann equation,^{23,24} and interface reflection and interference based on acoustic wave propagation²⁵ have been developed to model the thermal conductivity in superlattices. Due to their anisotropic structure, superlattices are expected to have anisotropic properties.⁸ However, most experimental thermal conductivity studies on superlattices are carried out in one direction only, particularly the cross-plane direction (perpendicular to the superlattice plane).^{9–15}

In this communication, we report the first experimental study on the temperature dependent anisotropic thermal conductivity in superlattices. Two Si/Ge superlattice samples with different structures were investigated. One is a Ge quantum-dot superlattice with silicon spacers and the other is a symmetrically strained Si/Ge superlattice. Both samples were grown by solid source molecular beam epitaxy (MBE). The quantum-dot superlattice, labeled

JL183, was grown on a Si(100) substrate at 540 °C. The growth rates for Si and Ge were 1 and 0.2 Å/s, respectively. The sample has a 500 Å Si buffer layer, followed by 50 bilayers, in which 1.5 nm Ge layers were separated by 20 nm Si spacer layers. Germanium dots were formed after self-assembly. The dot structure was investigated by transmission electron microscope and atomic force microscope (AFM). Figure 1a shows the equivalent first 10-layer cross section TEM image and Figure 1b shows the AFM image of the top layer. The typical dot size is determined to be 75 nm in base diameter and 7 nm in height. The dot density and nonuniformity are $2 \times 10^9 \text{ cm}^{-2}$ and 19%, respectively, as checked by AFM. The Ge wetting layer is about 6 Å. The total thickness of the Ge dot superlattice film is 1.06 μm. The Si/Ge symmetrically strained superlattice, labeled JL215, was grown on a silicon-on-insulator (SOI) substrate. The purpose of using a SOI rather than a Si wafer as a substrate is to facilitate the characterization of the electric and thermoelectric properties on the sample.²⁶

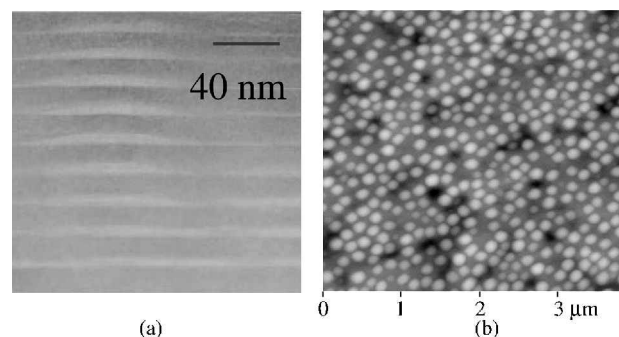


Fig. 1. Microscopic pictures of Ge dot samples: (a) cross-section TEM image of the equivalent first 10 layers; (b) AFM image of the top surface.

*Author to whom correspondence should be addressed.

To obtain the symmetrically strained Si/Ge superlattice, a SiGe alloy buffer layer was grown first to accommodate the lattice mismatch between the Si and the Ge. The buffer part of JL215, prepared by a surfactant mediation technique,²⁷ consists of a 500 Å Si layer, followed by a 1 μm continuously graded $\text{Si}_{1-x}\text{Ge}_x$ alloy layer with x increasing from 0 to 0.5, and a 0.3 μm $\text{Si}_{0.5}\text{Ge}_{0.5}$ alloy layer. The superlattice part, a 300-period $\text{Si}(20 \text{ \AA})/\text{Ge}(20 \text{ \AA})$ layer, was grown at 350 :C and doped to about $1 \times 10^{19} \text{ cm}^{-3}$ using Sb as a dopant. After the growth, the sample was annealed at 580 :C for 10 min to activate the dopant. At this doping level, the electron contribution to thermal conductivity is expected to be much smaller than that from lattice vibration according to the Wiedeman–Franz law and the measured electrical conductivity.¹³ The total thickness of the superlattice layer is 1.2 μm . An identical buffer, labeled JL214, was grown on the same SOI substrate and was used as the reference for JL215 in differential 3ω measurements. Generally, in Si/Ge superlattices grown by current MBE technology, interdiffusion between Si and Ge interfaces always occurs due to annealing.²⁸ The relatively low growth temperature (350 :C) of the superlattice can reduce interdiffusion and obtain a sharper interface.

The thermal conductivity values of the superlattices were measured by the 3ω technique, which is widely used in cross-plane thin-film thermal conductivity measurements.²⁹ Based on the same principle, the two-wire differential 3ω technique, which is used in this study, was developed to measure both the in-plane and cross-plane thermal conductivities.³⁰ A similar technique has been applied to investigate thermal conduction in polymer films.³¹ For the purpose of differential measurements, we prepared a Si reference sample for JL183 and an SOI reference sample for JL214 and JL215. On all five samples, an $\sim 100 \text{ nm}$ SiN_x layer was deposited by plasma enhanced chemical vapor deposition to provide electrical insulation for the measurement. On top of the SiN_x layer, two metallic 3ω heater–thermometer wires, with widths of 2 and 30 μm , respectively, were patterned and fabricated by electron-beam evaporation and lift-off technique. The 3ω measurements on both wires were conducted inside a vacuum cryostat that operated from 80 to 300 K. For the Ge dots sample JL183, the temperature drop across the superlattice layer for both 2 and 30 μm wires were obtained by subtracting the temperature rise data of JL183 from that of its reference Si sample, as shown in Figure 2, which demonstrates an example of experimental data of temperature rise measured at 80 K for 2 and 30 μm wires. After subtraction, a fitting program based on the two-dimensional heat conduction model³⁰ was used to find the in-plane thermal conductivity K_x and the cross-plane thermal conductivity K_y . Figure 2 also shows a comparison between experimental temperature rise data (points) and

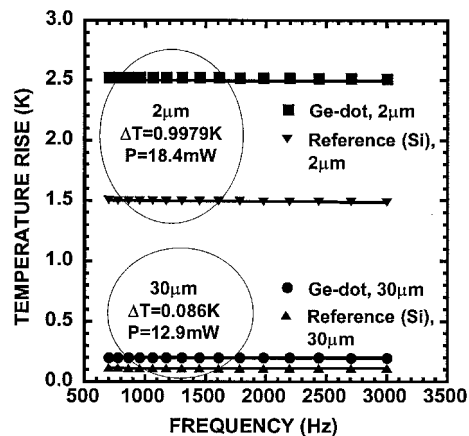


Fig. 2. Experimental temperature rise (represented by points) as a function of modulation frequency at 80 K on 2 and 30 μm heater wires for the Ge dots sample and the reference Si sample, compared with fitting results (represented by lines).

data obtained from the fitted results (lines). For superlattice sample JL215, a similar procedure was followed except that a two-step subtraction and fitting procedure was required to obtain K_x and K_y for the superlattice layer. The first step is to subtract the data of buffer sample JL214 from that of the reference SOI sample and fit the properties of the buffer layer. The second step is to subtract the data of superlattice sample JL215 from that of JL214 and fit the properties of the superlattice layer. After data processing, error analysis was carried out. The smaller is the thin-film thermal conductivity, the smaller is the uncertainty. For the quantum dots sample, the uncertainties in the in-plane and cross-plane directions are 30 and 25%, respectively. For the strained superlattice sample, the corresponding values are 20 and 10%.

The in-plane and cross-plane thermal conductivities of the two samples are plotted in Figures 3a and 4a. These data are compared with the expected values based on the bulk properties of Si and Ge, and the Fourier law in Figures 3b and 4b in logarithm scale. The figures show that both K_x and K_y of the two samples are appreciably reduced compared to the effective thermal conductivity values of those structures derived from their corresponding bulk values. The room-temperature in-plane thermal conductivity values of both superlattices are comparable to those of their corresponding compositionally equivalent alloy and the room-temperature cross-plane values are significantly lower than that of the alloy. The temperature dependence behaviors in the in-plane and cross-plane directions are different. In the cross-plane direction, thermal conductivity values for both samples increase monotonically with increasing temperature in the studied range. In the in-plane direction, there is an apparent “peak” on the $K_x - T$ curve between 100 and 150 K for JL183. This is similar to the peak thermal conductivity in bulk materials that usually is observed around

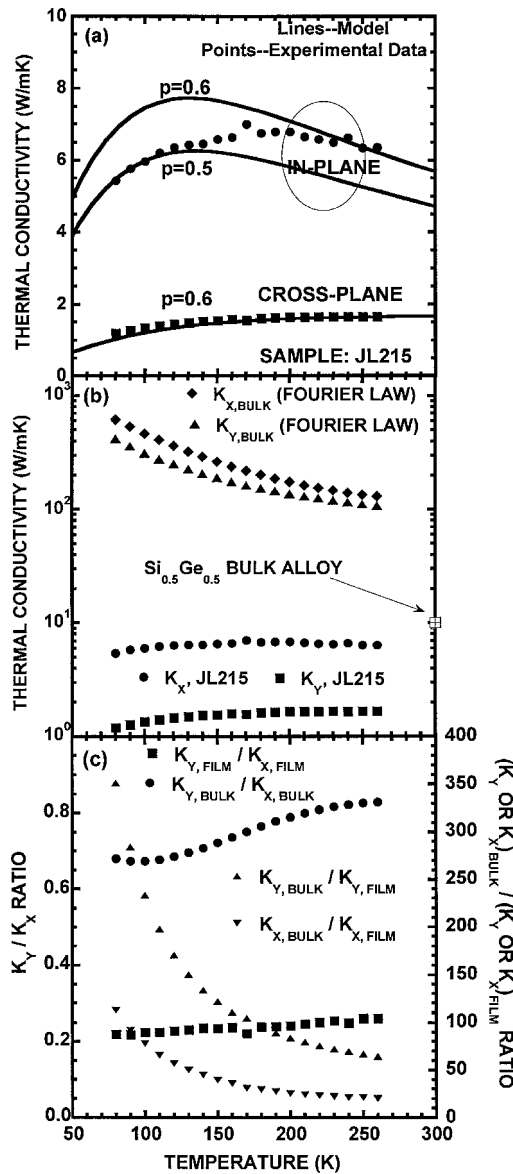


Fig. 3. Anisotropic thermal conductivity of the strained Si/Ge (20 Å/20 Å) superlattice: (a) experimental data and fitting based on Chen’s models (Refs. 23 and 24); (b) comparison of experimental data with predictions of Fourier theory based on bulk properties of each layer and with compositionally equivalent alloy (300 K); (c) ratio of K_y/K_x , and ratio of $K_{y,bulk}/K_{y,fil}$ and $K_{x,bulk}/K_{x,fil}$.

10–20 K. For JL215, K_x increases with increasing temperature up to about 200 K and then shows a slight downward trend. In Figures 3c and 4c, we plot the ratio of K_y/K_x obtained from experiments and compared with that expected from the Fourier theory using bulk thermal conductivity. Also in these figures are the relative reductions, shown as $K_{x,bulk}/K_{x,fil}$ and $K_{y,bulk}/K_{y,fil}$ ratios, in the in-plane and the cross-plane directions. Thermal conductivity reduction in the cross-plane direction can be 20–400 times and in the in-plane direction can be ~5–100 times, depending on temperature and material structure. Lattice

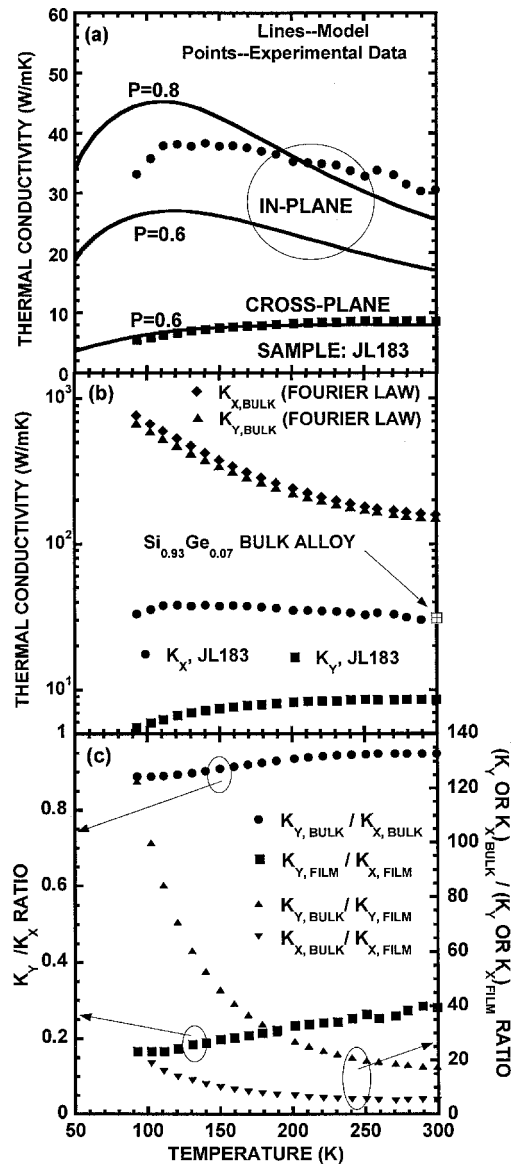


Fig. 4. Anisotropic thermal conductivity of the Ge-quantum dot sample: (a) experimental data and fitting based on Chen’s models (Refs. 23 and 24); (b) comparison of experimental data with predictions of Fourier theory based on bulk properties of each layer and with compositionally equivalent alloy (300 K); (c) ratio of K_y/K_x , and ratio of $K_{y,bulk}/K_{y,fil}$ and $K_{x,bulk}/K_{x,fil}$.

dynamics models^{17–19} for the cross-plane direction, considering the change in the phonon density of states and the group velocity reduction, predicts a thermal conductivity reduction of 6~7 times and ~30% in the cross-plane and in-plane directions at room temperature, respectively, which do not agree with experimental observation, especially along the in-plane direction.

To explain the experimental data, we used models developed by Chen based on the Boltzmann transport equation (BTE) for both in-plane²³ and cross-plane²⁴ directions. The models consider the possibility that some

phonons are diffusely scattered at the interfaces and employ a specular parameter p to represent the fraction of specularly scattered phonons. The models were developed for superlattice structures. The quantum-dot superlattice differs from this picture mainly in that the two interfaces within one period are not the same, whereas Chen's models assumed them to be identical, and the thickness of the Ge layer is not uniform. As a rough approximation, we applied the model to quantum-dot superlattices. In the modeling, we used the average thickness of the Si (200 Å) and Ge (15 Å) layers for JL183, and the exact period thickness of Si (20 Å) and Ge (20 Å) for JL215. The lines in Figures 3a and 4a were obtained from the model to capture the trend for the temperature dependent behavior along both in-plane and cross-plane directions. In the cross-plane direction, the models give excellent fits to the experimental data. The temperature dependence is mostly due to the specific heat of acoustic phonons, because the mean free path is limited by the film thickness. In the in-plane direction, the models can capture the trends of thermal conductivity peak and the correct order of magnitude of thermal conductivity reduction, but detailed agreements with experiments cannot be reached. Along the in-plane direction, phonons traveling along directions closely parallel to the interface are not disturbed, whereas those at a large angle are limited by the diffuse interface scattering. Thus the effective thermal conductivity still has features that reflect the presence of phonon-phonon scattering. These observations do affirm the conclusion that the diffuse interface scattering plays an essential role in the in-plane thermal conductivity reduction.

In summary, we have reported the first measurements of the temperature dependence of the anisotropic thermal conductivities of Si/Ge quantum-dot and strained superlattices. The results indicate a strong reduction in both in-plane and cross-plane thermal conductivities of the studied superlattices compared to Fourier theory values. These experimental results can be explained using theoretical models based on the Boltzmann transport equation that consider the partially diffuse scattering of the phonons at the superlattice interfaces. The study also indicated that the in-plane thermal conductivity can be reduced to the compositionally equivalent alloy level and the cross-plane thermal conductivity can be reduced much lower than that of the alloys.

Acknowledgment: This work was supported by a Department of Defense MURI program on thermoelectrics (N00014-97-1-0516).

References and Notes

1. G. Chen, *Ann. Rev. Heat Transfer* **7**, 1 (1996).
2. D. Hicks and M. S. Dresselhaus, *Phys. Rev. B* **47**, 12,727 (1993).
3. M. S. Dresselhaus, Y. M. Lin, S. B. Cronin, O. Rabin, M. R. Black, and G. Dresselhaus, *Semicond. Semimetals* **71**, 1 (2001).
4. T. C. Harman, P. J. Taylor, D. L. Spears, and M. P. Walsh, *J. Electron. Mater.* **29**, L1 (2000).
5. G. Chen, *Semicond. Semimetals* **71**, 203 (2001).
6. R. Venkatasubramanian, *Semicond. Semimetals* **71**, 175 (2001).
7. T. Yao, *Appl. Phys. Lett.* **51**, 1798 (1987).
8. G. Chen, C. L. Tien, X. Wu, and J. S. Smith, *J. Heat Transfer* **116**, 325 (1994).
9. X. Y. Yu, G. Chen, A. Verma, and J. S. Smith, *Appl. Phys. Lett.* **67**, 3554 (1995).
10. W. S. Capinski and H. J. Maris, *Physica B* **219**, 699 (1996).
11. W. S. Capinski, H. J. Maris, T. Ruf, M. Cardona, K. Ploog, and D. S. Katzer, *Phys. Rev. B* **59**, 8105 (1999).
12. S. M. Lee, D. G. Cahill, and R. Venkatasubramanian, *Appl. Phys. Lett.* **70**, 2957 (1997).
13. T. Borca-Tasciuc, W. L. Liu, J. L. Liu, T. F. Zeng, D. W. Song, C. D. Moore, G. Chen, K. L. Wang, M. S. Goorsky, T. Radeitic, R. Gronsky, T. Koga, and M. S. Dresselhaus, *Superlattices Microstruct.* **28**, 199 (2000).
14. R. Venkatasubramanian, *Phys. Rev. B* **61**, 3091 (2000).
15. D. W. Song, W. L. Liu, T. Zeng, T. Borca-Tasciuc, G. Chen, C. Caylor, and T. D. Sands, *Appl. Phys. Lett.* **77**, 3854 (2000).
16. S. Y. Ren and J. D. Dow, *Phys. Rev. B* **25**, 3750 (1982).
17. P. Hyldgaard and G. D. Mahan, *Phys. Rev. B* **56**, 10754 (1997).
18. S. Tamura, Y. Tanaka, and H. J. Maris, *Phys. Rev. B* **60**, 2627 (1999).
19. B. Yang and G. Chen, *Microscale Thermophys. Eng.*, to appear.
20. W. Bies, R. Radtke, and H. Ehrenreich, *J. Appl. Phys.* **88**, 1498 (2000).
21. A. Balandin and K. L. Wang, *Phys. Rev. B* **58**, 1544 (1998).
22. A. Khitun, A. Balandin and K. L. Wang, *Superlattices Microstruct.* **26**, 181 (1999).
23. G. Chen, *J. Heat Transfer* **119**, 220 (1997).
24. G. Chen, *Phys. Rev. B* **57**, 14958 (1998).
25. G. Chen, *J. Heat Transfer* **121**, 945 (1999).
26. T. Koga, S. B. Cronin, M. S. Dresselhaus, J. L. Liu, and K. L. Wang, *Appl. Phys. Lett.* **77**, 1490 (2000).
27. J. L. Liu, K. L. Wang, C. D. Moore, M. S. Goorsky, T. Borca-Tasciuc, and G. Chen, *Thin Solid Films* **369**, 121 (2000).
28. E. Kasper, Ed., *Properties of Strained and Relaxed Silicon Germanium*, *Electronic Material Information Service (EMIS) Datareviews Series*, No. 12, p. 47, INSPEC, the Institute of Electrical Engineers, (1995).
29. S. M. Lee and D. G. Cahill, *J. Appl. Phys.* **81**, 2590 (1997).
30. T. Borca-Tasciuc, A. R. Kumar, and G. Chen, *Rev. Sci. Instrum.*, **72**, 2139 (2001).
31. Y. S. Ju, K. Kurabayashi, and K. E. Goodson, *Thin Solid Films* **339**, 160 (1999).

Received: 8 February 2001. Revised: 26 March 2001.